# RADIATION CLIMATE MAP FOR ANALYZING RISKS TO ASTRONAUTS ON THE MARS SURFACE FROM GALACTIC COSMIC RAYS

*Premkumar B. Saganti*[1], *Francis A. Cucinotta*[2], *John W. Wilson*[3], *Lisa C. Simonsen*[3], and *Cary Zeitlin*[4]

[1]*Lockheed Martin Space Operations, Houston TX-77058;*
[2]*NASA Johnson Space Center, Houston, TX-77058;*
[3]*NASA Langley Research Center, Hampton, VA-23681*
[4]*Lawrence Berkeley National Laboratory, University of California, Berkeley, CA-94720*

## ABSTRACT

The potential risks for late effects including cancer, cataracts, and neurological disorders due to exposures to the galactic cosmic rays (GCR) is a large concern for the human exploration of Mars. Physical models are needed to project the radiation exposures to be received by astronauts in transit to Mars and on the Mars surface, including the understanding of the modification of the GCR by the Martian atmosphere and identifying shielding optimization approaches. The Mars Global Surveyor (MGS) mission has been collecting Martian surface topographical data with the Mars Orbiter Laser Altimeter (MOLA). Here we present calculations of radiation climate maps of the surface of Mars using the MOLA data, the radiation transport model HZETRN (high charge and high energy transport), and the quantum multiple scattering fragmentation model, QMSFRG. Organ doses and the average number of particle hits per cell nucleus from GCR components (protons, heavy ions, and neutrons) are evaluated as a function of the altitude on the Martian surface. Approaches to improve the accuracy of the radiation climate map, presented here using data from the *2001 Mars Odyssey* mission, are discussed.

## INTRODUCTION

The potential for harmful late effects including cancer, cataracts, neurological disorders, and non-cancer mortality risks, from galactic cosmic rays (GCR) pose a major threat for the human exploration of Mars [1-3]. Because of their high energies, the GCR are extremely penetrating and cannot be eliminated by practical amounts of shielding [4, 5]. The high charge and energy HZE ions portion of the GCR present unique challenges to biological systems such as DNA, cells, and tissue and the risks to humans is highly uncertain at this time [2, 5]. Another threat in deep space is solar particle events, which could induce acute radiation syndromes including death if the event is large enough and increase the risk of cancer or other late effects. However, shielding offered by the Mars atmosphere and spacecraft structures along with the early warning and detection systems may be effective as mitigation measures. The biological effects of protons are well understood being similar to gamma rays. Safety assurances and dose limits for the human exploration of Mars cannot be provided at this time due to the uncertainties in the biological effects of HZE ions [2]. Important physical data on the GCR elemental and energy composition near Mars and on the Mars surface will be needed prior to human exploration. Developing methods for the accurate prediction of the modulation of the isotopic composition and energies of the GCR after nuclear and atomic interactions with Mars atmosphere and soil and the accurate determination of secondary neutron spectra will be essential to design and undertake such missions.

Robotic precursor missions to Mars can provide valuable data on the radiation environment to be encountered in future human exploration missions of the red planet and validation of models used for mission design. These measurements should include direct physical measurements of the energy spectra of protons, heavy ions, and neutrons with radiation spectrometers. Physical data related to the Mars altitude [6], atmospheric, and soil composition will also be valuable in developing models of

astronaut and equipment exposures, and in designing shielded habitat configurations. In this paper, we discuss the use of the Mars Orbiter Laser Altimeter (MOLA) altitude data [6], and models of the radiation environment and GCR transport to present the first complete radiation map of the Mars surface.

## METHODS

The HZETRN (High Z and Energy Transport) code [4, 7] describes the atomic and nuclear reaction processes that alter the GCR in their passage through materials such as the Mars atmosphere and tissue. The HZETRN code solves the Boltzmann equation for the particle flux, $f_j(x,E)$, of ion of type $j$, with energy $E$, and depth $x$, as obtained from

$$\Omega \cdot \nabla f_j(x,\Omega,E) = \sum_k \int s_{jk}(\Omega,\Omega',E,E') f_k(x,\Omega',E') dE' d\Omega' - s_j(E) f_j(x,\Omega,E)$$

where $\sigma_j$ is the total reaction cross section and $\sigma_{jk}$ is the channel changing cross sections. The HZETRN code solves the Botzmann equation using the continuous slowing down approximation. The straight-ahead approximation is used for projectile nuclei [4] and angular dependence of scattering is considered for neutrons [7]. Details on the numerical methods used in this transport code can be found in refs. [4] and [ 7]. Nuclear fragmentation cross sections are described by the quantum multiple scattering (QMSFRG) model [8, 9]. The QMSFRG model considers the energy dependence of the nucleus-nucleus interaction, quantum effects in nuclear abrasion, and a stochastic model of the de-excitation of pre-fragment nuclei produced in projectile-target nuclei interactions. The organ dose equivalent, $H_T$ can be determined by integrating the particle energy spectra folded with the energy, mass, and charge dependent stopping power or linear energy transfer (LET), $L(E)$, and the LET dependent quality factor, $Q(L)$, and by considering the distribution of shielding at the tissue,

$$H_T = \sum_j \int dE\, f_j(E)\, L(E) Q[L(E)]$$

The organ dose equivalent, $H_T$ is expressed in the units of Sievert (Sv) (1 cSv = 1 rem). Values of the LET dependent $Q$ vary between 1 and 30 for the GCR with the highest values for LET = 50-200 keV/μm in the range of GCR ions with charge, Z=14-26.

The modulation of the GCR near Earth is described using the Badhwar *et al.,* [10, 11] model in terms of the magnetic field deceleration parameter, Φ. GCR spectra for several solar maximum (Φ = 1060 - 1216 MV) and solar minimum (Φ = 428 MV) scenarios were generated. Differences in solar modulation and GCR composition near-Earth and near-Mars have not been considered in the calculations. Webber [12] has estimated an increase in the modulation potential Φ of 10 MV per A.U., which suggests the change in GCR between Earth (~1.0 AU) and Mars (~1.5 AU) would be small, however the modulation would be in the energy region where HZE particles have maximum biological quality factors and confirmation of the change due to modulation is needed for human exploration. The simultaneous observation of GCR near-Earth and in Mars orbit is one approach to investigate the effects of the radial gradient on GCR. Energy spectra for the six most abundant GCR elements are fit to satellite data (H, He, C, O, Si, and Fe). The other GCR ions are scaled using values in the literature as described previously (ref. [11] and references cited therein).

The number of particle-hits per cell nucleus due to direct particle traversals [13] is evaluated using an average cell cross-sectional area of 100 $\mu m^2$. Calculations that include indirect cell hits from delta rays (secondary electrons) produced by ions will be reported elsewhere. Also, any additional shielding advantage from the Martian

surface magnetic fields (assumed to be weak and sparse at this time) will be addressed and reported in future when such data is available.

Low and high-density Mars atmospheric models (16 and 22 g/cm$^2$), assuming a spherically distributed $CO_2$ atmosphere, are considered for all calculations [14]. However, for simplicity, in this report only the high-density model (22 g/cm$^2$) calculations are presented. Atmospheric density is known to vary inversely with respect to the altitude from the mean surface. Based on the NASA published data [15], we have derived a model to assess the variation in the atmosphere with respect to the altitude. **Figure-1** plots $CO_2$ density versus altitude on the Mars surface for the low- and high-density models. **Figure-2** describes the geometry used in the calculations. Seasonal variations of atmospheric density are not included in these calculations and hence we refer to as the static atmospheric density model in our calculations.

The resultant shielding offered by the $CO_2$ atmosphere at a given altitude location is calculated for a set of geodesic distributed rays using the relation

$$s(z,q) = \sqrt{(R+h)^2 \cos^2(q) + \left[2R(z-h) + z^2 - h^2\right]} - (R+h)\cos(q)$$

where, *h* is the altitude above the mean surface, *s* being the distance along the slant path with zenith angle, ? (is calculated between 0 and $90^0$ with $1^0$ increments) and *z* is the vertical length of the atmosphere above the identified location. Radiation transport along the rays are then evaluated using the HZETRN code and results integrated over *z* and *h* to obtain particle flux at each location on the Martian surface.

Calculations of radiation transport in the human body, which locate astronauts at specific surface locations on Mars, were performed using the methods described in conjunction with computerized anatomical models [16] to represent the self-shielding of the human body. Particle energy spectra, organ dose equivalent, and cell hits were

evaluated at 12 representative different anatomical locations for solar minimum and solar maximum. Visualization of the Martian surface data was accomplished using the computer routines (VIZ-MARS) that we have developed for this application using the software package *MATLAB*.

## RESULTS AND DISCUSSION

By combining the organ dose equivalent with age and gender specific risk coefficients, an estimate of the probability of fatal cancer from radiation exposure is made [2, 5]. We note that the HZETRN model has been shown to predict the GCR dose equivalent to within ±25% accuracy. However, a much larger uncertainty exists in the understanding of the radiobiology of radiation effects at low dose-rates and of cancer risks from heavy ions [2, 5]. Estimates of cell damage [17, 18] have been considered along with the current organ dose equivalent to illustrate the role of attenuation of heavy ions by shielding such as the Martian atmosphere, spacecraft, and tissue shielding.

The major physical processes that modulate the heavy ions are atomic energy loss processes that are well described by stopping powers, and nuclear reactions including fragmentation and production processes [4, 8, 19]. **Figure-3a** shows calculations of the probability that a GCR ion will suffer a nuclear collision per cm of path-length in water. **Figure-3b** shows the elemental distribution of the GCR and calculations of the number of nuclear reactions made by each GCR charge group per path-length in water. These results illustrate that a large number of interactions of the GCR will occur with both tissue and the Mars atmosphere. However, the level of shielding provided is insufficient to completely eliminate the heavy ion components and also an accurate description of both fragmentation and transport is needed.

In **Figure-4** we show results for the number of particle hits per cell as a function of altitude on the Mars surface for distinct charge groups at solar minimum and solar maximum conditions. The number of cell hits by light ions such as protons and helium are only modestly affected by atmospheric shielding (altitude variations). This is due to the changes in the balance of loss from atomic slowing down processes and gain from the fragmentation of heavy ions or production from atoms in the atmosphere. In contrast, heavy ions undergo a large reduction with increasing atmosphere (decreasing altitude). In the present model we also predict that a significant contribution of heavy ion component occurs, especially at higher altitudes. Neutrons (not shown here) are less sensitive to changes in the amount of atmosphere since they contain an important back-scattered component at lower energies (< 100 MeV) [7]. Because neutrons will make up a larger contribution at low altitudes and production cross sections for neutrons are sensitive to target mass, information on atmospheric and soil composition will be important for designing surface habitats for astronauts. The *2001 Mars Odyssey* spacecraft [20] and future Lander missions should provide such data. **Figure-5** and **Figure-6** show results for the Martian radiation climate over the surface of Mars for protons and heavy ions respectively with both solar minimum and maximum conditions. These results indicate significant reduction for heavy and medium ions, moderate reduction for light ions, and little or no reduction for protons and neutrons (neutrons are not shown). Because of the large uncertainties in the biological effects of heavy ions, validation of these results by measurements on the surface of Mars will be essential for future human safety.

**Table-1** compares the organ dose equivalent en-route to Mars and **Table-2** on the Mars surface for the major tissues that contribute to radiation cancer risks during a solar minimum condition. Included in these calculations are results that consider the addition of shielding configurations of 5 or 10 cm of water equivalent material. The cruise phase of the mission could lead to organ doses that approach or exceed legal exposure limits used in low Earth orbit (LEO), which correspond to an excess

probability of 3% fatal cancer [21]. Dose limits are age and gender dependent as determined by epidemiology data. For manned exploration of Mars two types of missions are considered; conjunction-class where the mid-point of the mission is closer to Mars (Mars is on the same side of the Earth from Sun) and opposition-class where the mid-point is further from Mars (Mars is on the opposite side of the Earth from Sun). Conjunction-class missions involve longer stay on Mars (300-600 days) with one-way transit times of 150-250 days. Opposition-class missions involve shorter stay on Mars (20-60 days) with one-way transit times of 100-400 days [23]. The opposition-class missions require higher energy requirements. **Table-3** shows calculations of fatal cancer probabilities for 40-year-old males and females for such scenarios [5]. The 95% confidence levels shown are based on calculations, which consider the uncertainties in epidemiological data, radiation qualities, and the understanding of the physical environment. In **Table-3** the comparison with the addition of 10 cm water-shielding shows that the addition and optimization of shielding could lower risks to a level within the acceptable level of risk for LEO astronauts. However, the large uncertainties limit any conclusion on the acceptability of risk for long missions (> 100 d). The comparison in **Table-3** show that maximizing crew times on the Mars surface (conjunction-class missions) because of the lower surface doses will be favorable for human exploration. In **Figure-7** we show a climatic map of the skin dose equivalent for the entire surface of Mars. Variations on the order of 50% are predicted due to changes in atmosphere. Although, uncertainties in heavy ion radiobiology including the radiation quality factors are expected to be much larger at this time than estimates of physical quantities, a validation of the radiation climate map described here is needed. Surface validation measurements should include measurements of LET spectra and the integral dose and dose equivalent [20] along with spectroscopic data on neutrons.

## CONCLUSIONS

Calculations of the Martian radiation climate illustrate the level of detail that is now available by the most recent computer codes developed by NASA. Critical questions to be addressed include what is the current accuracy of these calculations, what accuracy will be required, and what measurements are needed to validate these models? Previous comparisons with measurements near Earth provide some validation of the models used here and an agreement to within 25% is found for the dose equivalent. However, clearly data near Mars and most importantly on the surface of Mars will be needed in the context of the high level concern of biological risks to astronauts from heavy ions. At present, NASA Johnson Space Center's MARIE (Martian Radiation Environment Experiment) instrument on board the *2001 Mars Odyssey* spacecraft has been collecting and successfully providing data for the Martian radiation environment mapping since March 13, 2002 [24]. In near future, other radiation instruments are being planned to land on Martian surface and provide similar data. Once these measurements are available, they will be utilized to verify our calculated predictions and update the models as needed. Local measurements on Martian surface including atmospheric density variations and regolith contributed *albedo* radiation will be valuable for designing future human exploration missions to Mars.

## REFERENCES


1. National Academy of Sciences Space Science Board, HZE Particle Effects in Manned Space Flight, National Academy of Sciences U.S.A. Washington D.C., 1973.

2. National Academy of Sciences, NAS. National Academy of Sciences Space Science Board, Report of the Task Group on the Biological Effects of Space Radiation. Radiation Hazards to Crews on Interplanetary Mission National Academy of Sciences, Washington, D.C., 1997.

3. Cucinotta, F.A., Manuel, F.K., Jones, J., Izsard, G., Murray, J., Djojenegoro, and Wear, M., Space Radiation and Cataracts in Astronauts. *Radiat. Res.* **156**, 460-466 2001.

4. Wilson J.W., Townsend, L.W., Schimmerling, W., Khandelwal G.S., Khan, F., Nealy, J.E., Cucinotta, F.A., Simonsen, L.C., and Norbury, J.W., Transport methods and interactions for space radiations, NASA-RP**1257**, 1991.

5. Cucinotta, F.A., Schimmerling, W., Wilson, J.W., Peterson, L.E., Badhwar, G.D., Saganti, P., and Dicello, J.F., Space Radiation Cancer Risks and Uncertainties for Mars Missions. *Radiat. Res.* **156**, 682-688, 2001.

6. Smith, D.E., Zuber, M.T., Solomon, S.C., Philips, R.J., Head, J.W., Garvin, J.B., et al., The Global Topography of Mars and Implications for Surface Evolution. *Science* **284**, 1495-1503, 1999.

7. Clowdsley, M.S., Wilson, J.W., Kim, M., Singleterry, R.C., Tripathi, R.K., Heinbockel, J.H., Badavi, F.F., and Shinn, J.L., Neutron Environments on the Martian Surface. *Physica Medica* **17**, 94-96, 2001.

8. Cucinotta, F.A., Wilson, J.W., Tripathi, R.K.; and Townsend, L.W., Microscopic, Fragmentation Model For Galactic Cosmic Ray Studies. *Adv. in Space Res.* **22**, 533-537, 1998.

9. Cucinotta, F.A., Wilson, J.W., Shinn, J.L., Tripathi, R.K., Maung, K.M., Badavi, F.F., Katz, R., and Dubey, R.D.: Computational Procedures and Data-Base Development. In: NASA Workshop on Shielding Strategies for Human Space Exploration. Eds. Wilson, J.W., Miller, J., Konradi, A., and Cucinotta, F.A., NASA CP-**3360**, 1997.

10. Badhwar, G.D., and O'Neill, P.M., An Improved Model of GCR for Space Exploration Missions. *Nucl. Tracks Radiat. Meas.* **20**, 403-410, 1992.

11. Badhwar, G. D., Cucinotta, F. A., and O'Neill, P. M.: An Analysis of Interplanetary Space Radiation Exposure for Various Solar Cycles. *Radiat. Res.* **138**, 201-208, 1994.

12. Webber, W. R., The Interstellar Cosmic Ray Spectrum and Energy Density. Interplanetary Cosmic Ray Gradients and a New Estimate of the Boundary of the Heliosphere. *Astron. Astrophys.* **179**, 277-284, 1987.

13. Cucinotta F.A., Nikjoo H., and Goodhead D.T., The Effects of Delta Rays on The Number of Particle-Track Traversals per Cell in Laboratory and Space Exposures. *Radiat. Res.* **150**, 115-119, 1998.

14. Simonsen, L.C., Wilson, J.W., Kim, M.H., and Cucinotta, F.A., Radiation Exposure for Human Mars Exploration. *Health Phys*. **79**, 515-525, 2000.

15. Simonsen L.C., Analysis of Lunar and Mars Habitation Modules for the Space Exploration Initiative, Chapter-4 in Shielding Strategies for Human Space Exploration, Ed. J. W. Wilson, J. Miller, A. Konradi, and F. A. Cucinotta, NASA CP-**3360**, 43-77, 1997

16. Billings, M.P., Yucker, W.R., and Heckman, B.R., Body Self-Shielding Data Analysis, McDonald Douglas Astronautics Company West, MDC-**G4131**, 1973.

17. Cucinotta, F.A., Wilson, J.W., Katz, R., Atwell, W., and Badhwar, G. D., Track Structure and Radiation Transport Models for Space Radiobiology Studies. *Adv. in Space Res.* **18**, 183, 194-203, 1995.

18. Cucinotta, F.A., and Dicello, J.F., On the Development of Biophysical Models for Space Radiation Risk Assessment. *Adv. Space. Res.* **25**, 2131-2140, 2000.

19. Zeitlin, C., Heilbronn, L., Miller, J., Rademacher, S.E., Borak, T., Carter, T.R., Frankel, K.A., Schimmerling, W., and Stronach, C.E., Heavy Fragment Production Cross Sections for 1.05 GeV/nucleon $^{56}$Fe in C, AL, Cu, Pb, and $CH_2$ Targets. *Phys. Rev. C* **56**, 388-397, 1997.

20. References this special issue.

21. National Council on Radiation Protection and Measurements, Radiation Protection Guidance for Activities in Low Earth Orbit, NCRP Report **132**, Bethesda MD, 2000.

22. Badhwar, G., this special issue.

23. Cucinotta, F. A., Badhwar, G. D., Saganti, P. B., Schimmerling, W., Wilson, J.W., Peterson, L., and Dicello, J., Space Radiation Cancer Risk Projections for Exploration Missions: Uncertainty Reduction and Mitigation, NASA TP-**21077**, 2002.

24. For more info http://srhp.jsc.nasa.gov/ and http://marie.jsc.nasa.gov/

**Table-1**: The effectiveness of water shielding (5 g/cm$^2$ and 10 g/cm$^2$) in transit form Earth to Mars on the organ dose equivalent at 12 different locations in the human body during solar minimum condition. The "Point" dose refers to dose without body shielding and the "Skin" organ location refers to the average dose in the human body at the skin level.

| | *Organ Dose Equivalent (cSv/yr)* | | | | |
|---|---|---|---|---|---|
| *Organ* | *0 cm* | *5 cm* | *10 cm* | *%Reduction by 5 cm* | *%Reduction by 10 cm* |
| Point | 120.0 | 95.6 | 74.3 | 20.3 % | 38.1 % |
| Skin | 94.1 | 73.2 | 60.0 | 22.3 | 36.2 |
| Eye | 96.0 | 73.7 | 60.5 | 23.2 | 37.0 |
| BFO | 70.0 | 58.2 | 50.7 | 16.9 | 27.6 |
| Bladder | 60.1 | 52.0 | 46.7 | 13.5 | 22.4 |
| Colon | 69.0 | 57.7 | 50.5 | 16.4 | 26.9 |
| Esophagus | 65.9 | 55.6 | 48.9 | 15.6 | 25.7 |
| Gonads | 73.7 | 60.0 | 51.7 | 18.6 | 29.9 |
| Liver | 63.5 | 54.1 | 48.0 | 14.8 | 24.4 |
| Lung | 66.8 | 56.2 | 49.4 | 15.9 | 26.1 |
| Stomach | 61.0 | 52.6 | 47.1 | 13.7 | 22.7 |
| Thyroid | 72.6 | 59.8 | 51.8 | 17.6 | 28.7 |

**Table-2**: The effectiveness of water shielding (5 g/cm$^2$ and 10 g/cm$^2$) on the Mars surface for the organ dose equivalent at 12 different locations in the human body during solar minimum condition. The "Point" dose refers to the dose without body shielding and the "Skin" organ location refers to the average dose in the human body at the skin level.

| | *Organ Dose Equivalent (cSv/yr)* | | | | |
|---|---|---|---|---|---|
| *Organ* | *0 cm* | *5 cm* | *10 cm* | *%Reduction by 5 cm* | *%Reduction by 10 cm* |
| Point | 25.8 | 21.3 | 20.1 | 17.4 % | 22.1 % |
| Skin | 19.3 | 18.6 | 18.0 | 3.8 | 6.8 |
| Eye | 19.7 | 18.8 | 18.2 | 4.4 | 7.7 |
| BFO | 19.4 | 18.7 | 18.0 | 3.9 | 6.9 |
| Bladder | 21.1 | 19.7 | 18.9 | 6.4 | 10.5 |
| Colon | 19.2 | 18.5 | 18.0 | 3.6 | 6.5 |
| Esophagus | 19.1 | 18.5 | 17.9 | 3.4 | 6.2 |
| Gonads | 19.8 | 18.9 | 18.3 | 4.3 | 7.5 |
| Liver | 19.6 | 18.8 | 18.2 | 4.0 | 7.2 |
| Lung | 19.6 | 18.8 | 18.2 | 4.0 | 7.1 |
| Stomach | 21.1 | 19.8 | 19.0 | 6.1 | 10.2 |
| Thyroid | 19.0 | 18.3 | 17.8 | 3.4 | 6.1 |

**Table-3.** Percent excess fatal cancer risk projections and 95% C. I.'s for 40-year-old females or males. Calculations are for opposition or conjunction type Mars missions using 4 g/cm$^2$ aluminum shielding and high density Mars $CO_2$ atmosphere and considering effects of the addition of 10 cm water shielding. Values in parenthesis indicate days on Mars surface [5].

| *Mission Type* | *Days (Mars or lunar surface)* | *0 cm $H_2O$* | *10 cm $H_2O$* |
|---|---|---|---|
| | Females | | |
| Opposition | 360 (30) | 3.3 [0, 18.0] | 2.5 [0, 14.6] |
| Opposition | 660 (30) | 6.2 [0, 34.0] | 4.6 [0, 27.5] |
| Conjunction | 1000 (600) | 5.7 [0, 30.8] | 4.5 [0, 25.6] |
| | Males | | |
| Opposition | 360 (30) | 2.0 [0, 10.8] | 1.5 [0, 8.8] |
| Opposition | 660 (30) | 3.7 [0, 20.4] | 2.8 [0, 16.5] |
| Conjunction | 1000 (600) | 3.4 [0, 18.5] | 2.7 [0, 15.3] |

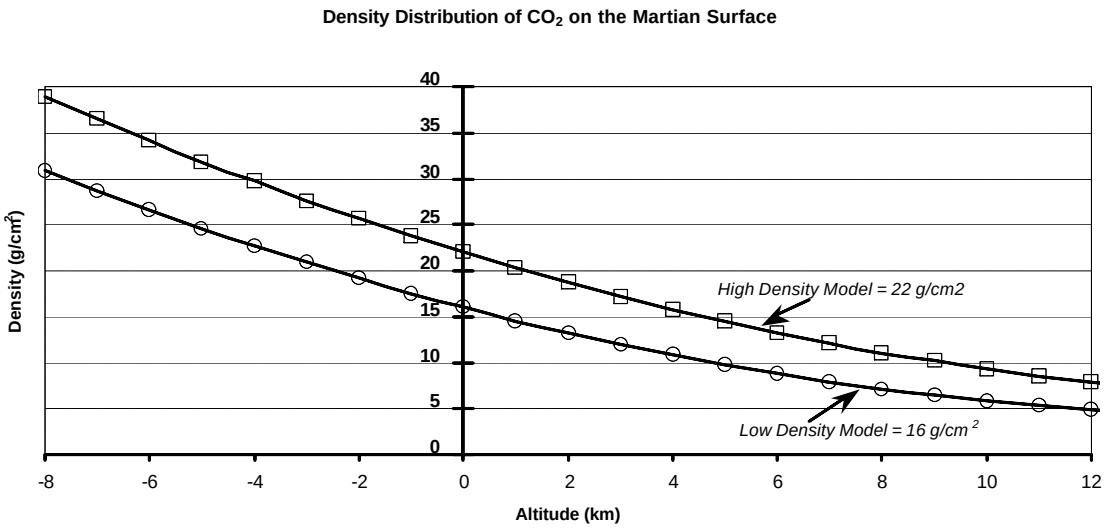


**Figure-1**: Density model of the $CO_2$ atmosphere on the Martian surface. The two density models, low-density (16 g/cm$^2$) and high-density (22 g/cm$^2$) are generally considered at the mean surface (0 km). The variation in the $CO_2$ density at a given altitude (-8 to +12 km) is derived, as shown in this figure, for both the density models from the NASA published data [15]. All particle flux calculations presented in this report are only for the high-density (22 g/cm$^2$) $CO_2$ model with altitude variation.

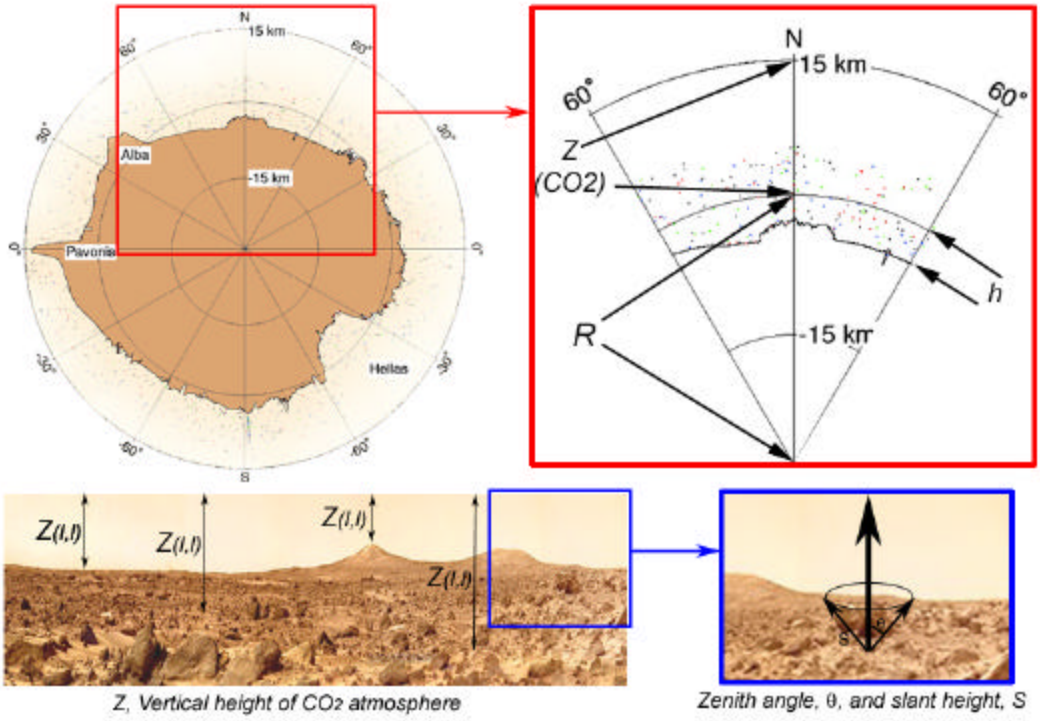


**Figure-2.** Top left image is an illustration of the global profile of the Martian surface from data obtained by MOLA crossing longitudes 52°E and 247°E. The north and south polar caps are at the top and bottom with a vertical exaggeration of 100:1 (adopted from Smith et al. [6]). Top right is the description of the mean surface radius, R, vertical height, Z, of the $CO_2$ atmosphere above the mean surface, and height of the target point above / below the mean surface as used in the calculations. Bottom left is the Martian surface as seen from the Pathfinder landing site with the description of variations in the vertical height of the Martian atmosphere for a given longitude and latitude values, $Z_{(l,l)}$. Bottom right is the description of the slant height, s, and the zenith angle, ?, used in the calculations for the effective shielding from the atmosphere at a given target point on the Martian surface.

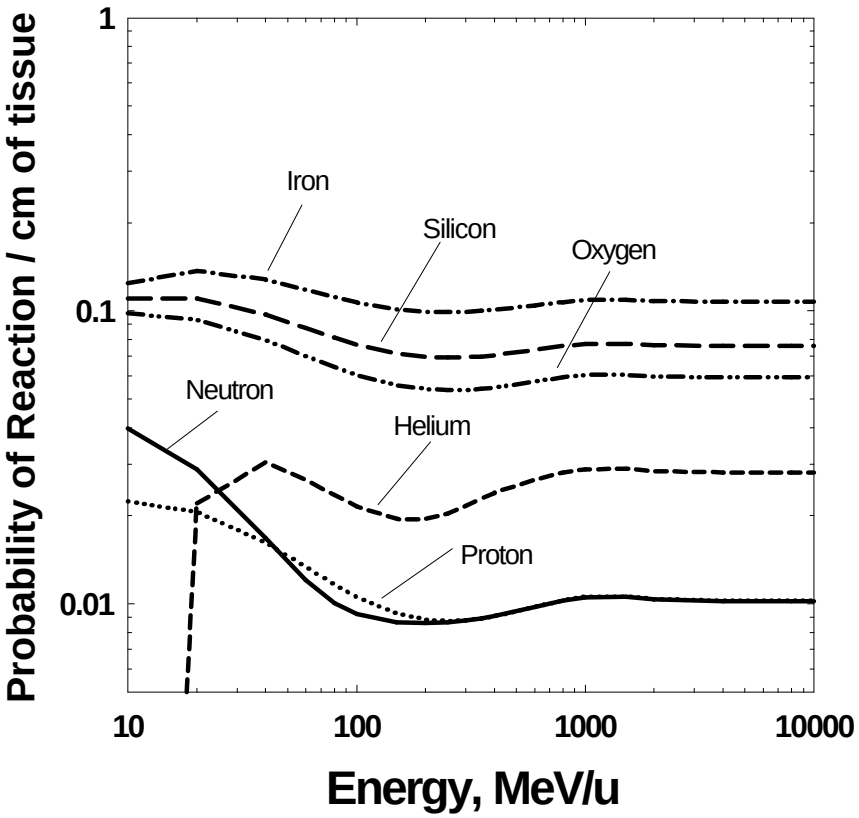


**Figure-3a.** The probability of a nuclear reaction per cm of tissue traversed versus energy for several ions prominent in the GCR.

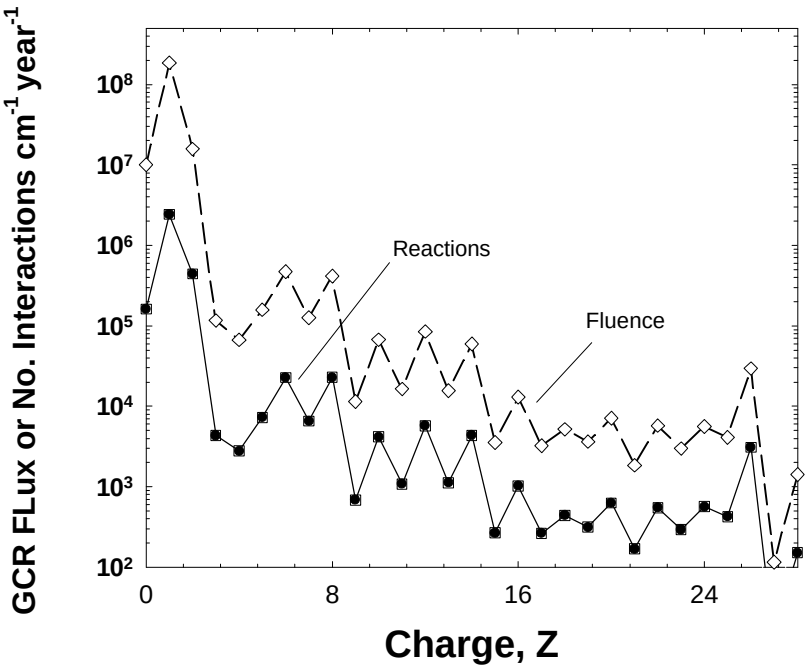


**Figure-3b.** Comparisons of the elemental fluence of GCR ions near solar minimum to the number of nuclear interactions that occur per cm of tissue traversed by each charge GCR group. Calculations are made behind 5 cm of tissue

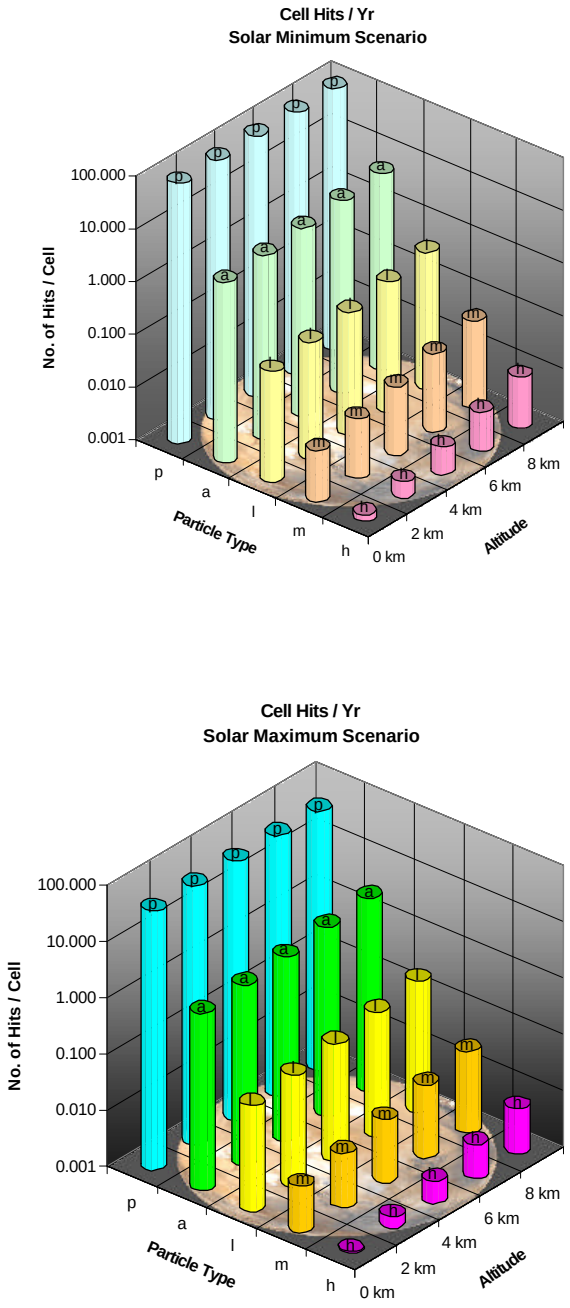


**Figure-4.** Comparison of calculated particle hits per cell per year at the skin on the Martian surface for solar minium and solar maximum conditions. Calculations include the average body shielding on the skin for the 50% percentile male [16]. Results for protons, alpha, light, medium, and heavy charge groups are shown

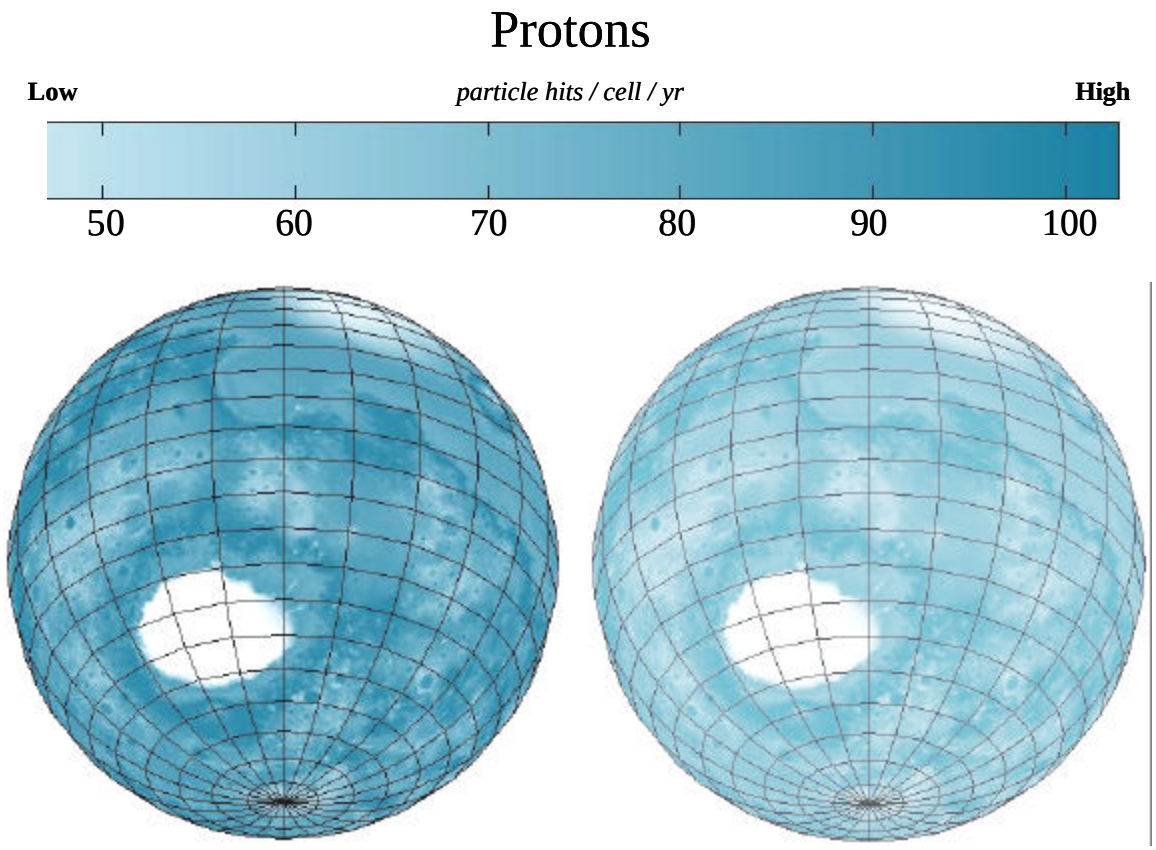


**Figure-5.** Estimates of the number of proton hits per cell per year on the Martian surface. Calculations consider the transport of the GCR through the Mars atmosphere using the MOLA topographical data and include the average body shielding on the skin for the 50% percentile male [16]. Calculations consider the extreme solar cycle scenarios with calculations with left panel near solar minimum (with solar deceleration parameter, $\Phi$ = 428 MV) and right panel solar maximum scenario ($\Phi$ = 1050 MV) is shown.

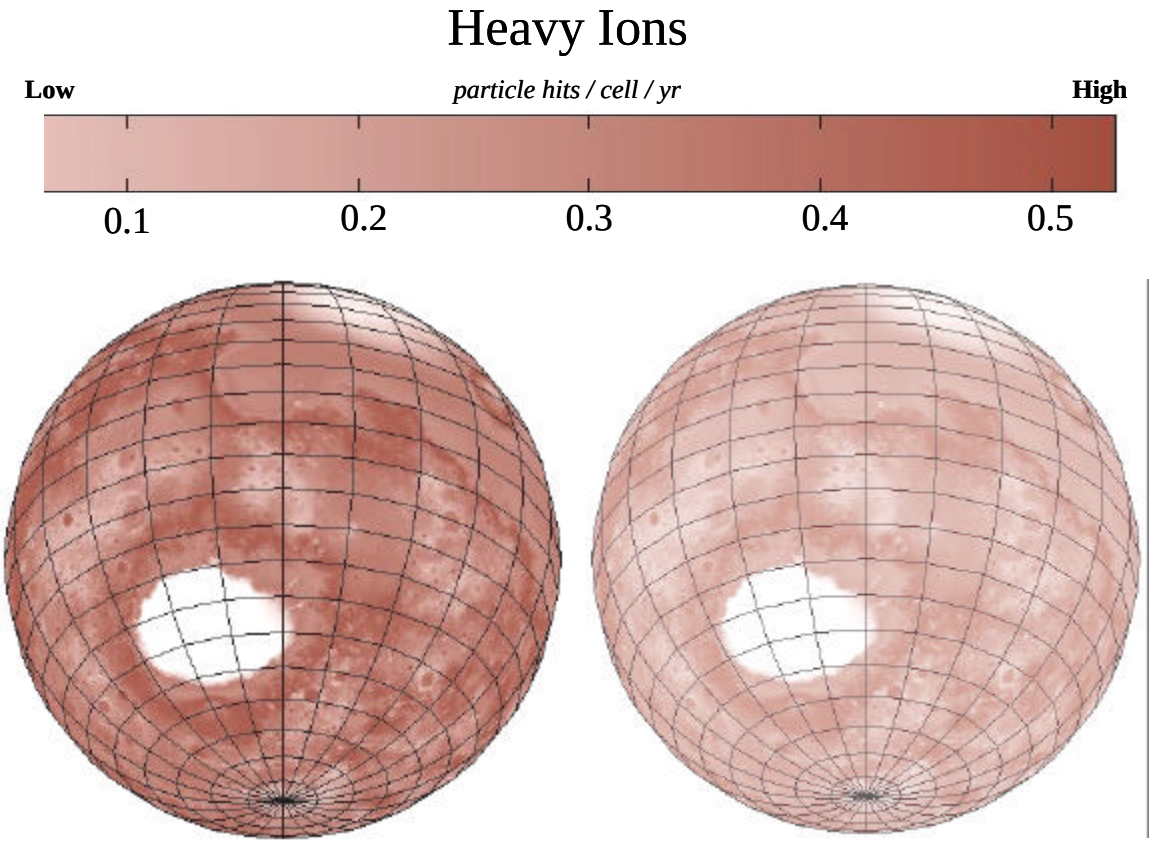


**Figure-6.** Estimates of the number of heavy ion (Z>2) hits per cell per year on the Martian surface. Calculations consider the transport of the GCR through the Mars atmosphere using the MOLA topographical data include the average body shielding on the skin for the 50% percentile male [16]. Calculations consider the extreme solar cycle scenarios with calculations with left panel near solar minimum (with solar deceleration parameter, $\Phi$ = 428 MV) and right panel solar maximum scenario ($\Phi$ = 1050 MV) is shown.

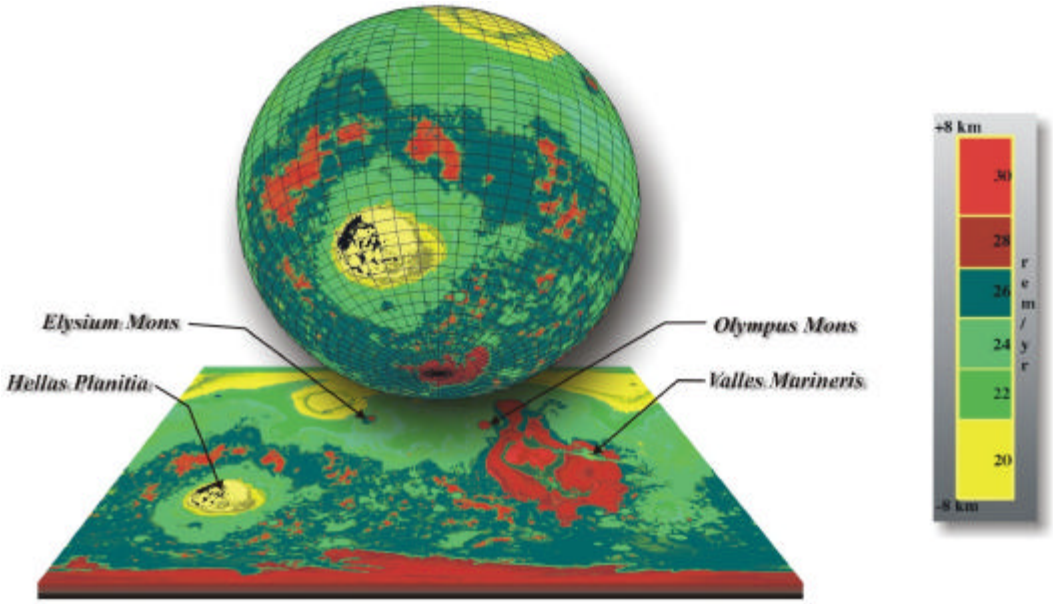


**Figure-7.** Calculations of the skin dose equivalent for astronauts on the surface of Mars near solar minimum. The variation in the dose with respect to altitude is shown. Higher altitudes (such as Olympus Mons) offer less shielding from the $CO_2$ atmosphere and lower altitudes (such as Hellas Planatia). The effective total dose has a range between 20 and 30 cSv/yr as a function of altitude for the static atmospheric high-density $CO_2$ model used here.